

Radio Science, Volume ???, Number , Pages 1–25,

¹ Accurate 2.5-D Boundary Element Method ² for Conductive Media

Dieter Dobbelaere,¹ Hendrik Rogier¹ and Daniël De Zutter¹

Corresponding author: D. Dobbelaere, Electromagnetics Group, Department of Information Technology, Ghent University, Sint-Pietersnieuwstraat 41, 9000 Ghent, Belgium.
(dieter.dobbelaere@intec.ugent.be)

¹Department of Information Technology,
Ghent University, Belgium.

3 The solution of the time-harmonic Maxwell equations using a boundary
4 element method, for 2-D geometries illuminated by arbitrary 3-D excitations,
5 gives rise to numerical difficulties if highly conductive media are present. In
6 particular, the interaction integrals arising in the method of moments involve
7 kernels that strongly oscillate in space and, at the same time, decay expo-
8 nentially. We present an accurate method to tackle these issues over a very
9 broad conductivity range (from lossy dielectric to conductor skin-effect regime),
10 for both magnetic and non-magnetic conductors. Important applications are
11 the modal analysis of waveguides with non-perfect conductors, scattering prob-
12 lems and shielding problems with enclosures with arbitrary permeability and
13 conductivity and 3-D noise sources.

1. Introduction

14 Boundary element methods (BEMs) provide a powerful framework to solve the
15 time-harmonic Maxwell equations numerically. If the problem domain consists of
16 homogeneous material regions, a BEM generally requires fewer unknowns than a vol-
17 umetric discretization technique. This paper considers two-dimensional geometries
18 with conductive material regions, which can be magnetic, illuminated by arbitrary
19 three-dimensional sources, leading to a so-called 2.5-D boundary element method.
20 Important applications of this class of problems are propagation in uniform waveg-
21 uides with non-perfect conductors [*Coluccini et al.*, 2013; *Tong et al.*, 2005; *Dobbe-*
22 *laere et al.*, 2013a], scattering problems [*Murphy et al.*, 1991] and shielding problems
23 [*Dobbelaere et al.*, 2013b].

24 Interaction integrals appearing in the method of moments (MoM), with the scalar
25 Green's function and its normal derivatives as kernels, are numerically challenging
26 due to two specific and interplaying aspects. First, the kernels in good conductors are
27 strongly oscillating and exponentially decaying in space, due to the large magnitude
28 and imaginary part of the conductor's wave number w.r.t. the free space wave number.
29 Second, the kernels are singular, or nearly singular, in those regions of the integration
30 domain where the test and basis functions' supports overlap or lie close to each other,
31 respectively. This behavior requires special care for an accurate numerical evaluation.
32 Moreover, the combination of the two aspects, i.e. interaction integrals with both
33 (nearly) singular and oscillating as well as exponentially damped integrands, poses

34 further difficulties. In this paper we present an accurate method to handle both
35 problems.

36 A large amount of literature is available concerning the numerical evaluation of
37 MoM interaction integrals in low-loss dielectric media. Integrals with singular or
38 nearly singular integrands are usually evaluated with a singularity extraction [*Wilton*
39 *et al.*, 1984; *Yla-Oijala and Taskinen*, 2003; *Graglia*, 1993] or cancellation technique
40 [*Khayat and Wilton*, 2005; *Graglia and Lombardi*, 2008; *Polimeridis and Mosig*, 2010].
41 In 3-D, *Chakraborty and Jandhyala* [2004] use singularity cancellation with RWG
42 basis functions [*Rao et al.*, 1982] to evaluate the interaction integrals in conductive
43 media more accurately. A good overview of the additional problems that arise in
44 conductive media can be found in *Peeters et al.* [2012], together with a singularity
45 cancellation technique for the three-dimensional case.

46 To the authors' best knowledge, no accurate method for handling interaction in-
47 tegrals in conductive media for the 2.5-D case has been presented yet. This work
48 proposes a new method specifically tailored to the properties of the 2.5-D Green's
49 function in conductive media. It is shown, both theoretically and through corrob-
50 orating examples, that the method accurately evaluates interaction integrals for a
51 wide range of electrical conductivities (low-loss dielectric to highly conductive) and
52 frequencies, and allows media with arbitrary permeability. In addition to the earlier
53 mentioned fields of application, the new method is highly relevant to the accurate
54 analysis of state-of-the-art multiconductor transmission lines and enclosures.

55 The structure of this paper is as follows: in Sections 2 and 3 we briefly outline the
 56 employed integral equations and the interaction integrals appearing in the MoM. The
 57 problems encountered in evaluating the integrals in conductive media are elaborated
 58 in Section 4, followed by our new method in Section 5. Finally, the numerical exam-
 59 ples in Section 6 testify to the accuracy and applicability of the method, and clearly
 60 demonstrate the advantages over existing methods. Conclusions are formulated in
 61 Section 7.

2. Geometry and Boundary Integral Equations

62 Consider a 2-D geometry consisting of isotropic homogeneous material regions Ω_i ,
 63 with permittivity $\epsilon_i \in \mathbb{C}$, permeability $\mu_i \in \mathbb{C}$ and boundary C_i (Fig. 1). Assume
 64 that all sources and fields have a common time and longitudinal dependence $e^{j(\omega t - \beta z)}$
 65 ($\beta \in \mathbb{C}$), which is omitted for notational convenience. A general 3-D excitation can
 66 be expanded into sources of this kind via Fourier transformation in the z direction.
 67 The unknowns of the problem are the tangential electric and magnetic boundary
 68 fields, given by $\hat{\mathbf{n}} \times \mathbf{E} \times \hat{\mathbf{n}} = E_t \hat{\mathbf{t}} + E_z \hat{\mathbf{z}}$ and $\hat{\mathbf{n}} \times \mathbf{H} \times \hat{\mathbf{n}} = H_t \hat{\mathbf{t}} + H_z \hat{\mathbf{z}}$, with E_t and H_t
 69 the transverse tangential components, and E_z and H_z the longitudinal components.
 70 The following representation formulas hold [*Olyslager et al.*, 1993], with $E_t^{(i)} \hat{\mathbf{t}} + E_z^{(i)} \hat{\mathbf{z}}$
 71 the incoming tangential electric field generated by sources in Ω_i , $\mathbf{r} = x\hat{\mathbf{x}} + y\hat{\mathbf{y}}$, and

$$\gamma_i = \sqrt{\omega^2 \epsilon_i \mu_i - \beta^2}:$$

$$E_z(\mathbf{r}) = E_z^{(i)}(\mathbf{r}) + \oint_{C_i} \left[E_z(\mathbf{r}') \frac{\partial G_i(\mathbf{r}|\mathbf{r}')}{\partial n'} - \left(\frac{j\gamma_i^2}{\omega\epsilon_i} H_t(\mathbf{r}') - \frac{\beta}{\omega\epsilon_i} \frac{\partial H_z(\mathbf{r}')}{\partial t'} \right) G_i(\mathbf{r}|\mathbf{r}') \right] dc', \quad (1)$$

$$E_t(\mathbf{r}) = E_t^{(i)}(\mathbf{r}) + \oint_{C_i} \left[\frac{j\omega\mu_i}{\gamma_i^2} H_z(\mathbf{r}') \frac{\partial^2 G_i(\mathbf{r}|\mathbf{r}')}{\partial n \partial n'} - \frac{j\beta}{\gamma_i^2} E_z(\mathbf{r}') \frac{\partial^2 G_i(\mathbf{r}|\mathbf{r}')}{\partial t \partial n'} + \frac{j\omega\mu_i}{\gamma_i^2} \left(\frac{j\gamma_i^2}{\omega\mu_i} E_t(\mathbf{r}') - \frac{\beta}{\omega\mu_i} \frac{\partial E_z(\mathbf{r}')}{\partial t'} \right) \frac{\partial G_i(\mathbf{r}|\mathbf{r}')}{\partial n} + \frac{j\beta}{\gamma_i^2} \left(\frac{j\gamma_i^2}{\omega\epsilon_i} H_t(\mathbf{r}') - \frac{\beta}{\omega\epsilon_i} \frac{\partial H_z(\mathbf{r}')}{\partial t'} \right) \frac{\partial G_i(\mathbf{r}|\mathbf{r}')}{\partial t} \right] dc'. \quad (2)$$

Similar expressions for the magnetic field components are found with the duality substitutions $E \rightarrow H$, $H \rightarrow -E$, $\epsilon_i \rightarrow \mu_i$ and $\mu_i \rightarrow \epsilon_i$ in (1) and (2). With the choice $G_i(\mathbf{r}|\mathbf{r}') = \frac{j}{4} H_0^{(2)}(\gamma_i |\mathbf{r} - \mathbf{r}'|)$, the Green's function satisfies the Sommerfeld radiation condition at infinity, provided the branch cuts of γ_i are chosen such that $\Im \gamma_i \leq 0$.

A system of coupled integral equations is obtained after imposing continuity of the tangential fields at the boundaries, yielding a 2.5-D version of the PMCHWT (Poggio-Miller-Chang-Harrington-Wu-Tsai) operator [Poggio and Miller, 1973; Chang and Harrington, 1977; Wu and Tsai, 1977]. A finite-dimensional linear system is obtained with the MoM.

3. MoM Interaction Integrals

Before presenting our new theory from Section 4 onwards, we briefly recall which type of interaction integrals occur in the MoM of the 2.5-D PMCHWT boundary integral equation [Olyslager et al., 1993; Fostier et al., 2011]. The boundaries C_i are meshed into a union of segments S_j with length l_j , separated by nodes \mathbf{r}_k (Fig. 2).

86 The transverse tangential components E_t and H_t are expanded in terms of pulse
 87 functions $p_j(\mathbf{r})$, with support over segment S_j , whereas the longitudinal components
 88 E_z and H_z are expanded into triangular functions $t_k(\mathbf{r})$, with support over segments
 89 that share a node \mathbf{r}_k [Olyslager et al., 1993; Fostier et al., 2011]:

$$\begin{aligned} p_j(\mathbf{r}) &= 1 & \mathbf{r} \in S_j, \\ t_k(\mathbf{r}) &= 1 - |\mathbf{r} - \mathbf{r}_k| l_j^{-1} & \mathbf{r}, \mathbf{r}_k \in S_j. \end{aligned} \quad (3)$$

90 The continuity equations for E_z and H_z are tested with pulse functions, whereas
 91 the equations for E_t and H_t are tested with triangular functions. To calculate the
 92 elements in the MoM system matrix, the interaction integrals (4)-(6) below need to
 93 be evaluated numerically for basis and test functions with support over segments
 94 that have Ω_i as a neighboring medium. This can easily be seen by inspecting (1) and
 95 (2). The tangential derivatives of the Green's function can be transferred to the test
 96 function using integration by parts such that only three types of interaction integrals
 97 remain:

$$I_{jk}^{(1)} = \int_{C_i} p_j(\mathbf{r}) dc \int_{C_i} G_i(\mathbf{r}|\mathbf{r}') p_k(\mathbf{r}') dc', \quad (4)$$

$$I_{jk}^{(2)} = \int_{C_i} p_j(\mathbf{r}) dc \int_{C_i} \frac{\partial G_i(\mathbf{r}|\mathbf{r}')}{\partial n'} t_k(\mathbf{r}') dc', \quad (5)$$

$$I_{jk}^{(3)} = \int_{C_i} t_j(\mathbf{r}) dc \int_{C_i} \frac{\partial^2 G_i(\mathbf{r}|\mathbf{r}')}{\partial n \partial n'} t_k(\mathbf{r}') dc'. \quad (6)$$

4. Difficulties in Conductive Media

98 Consider a conductive region Ω , with conductivity σ , complex permittivity $\epsilon =$
 99 $\epsilon_0 - j \frac{\sigma}{\omega}$ and permeability μ . The transversal wave number γ can be written as a
 100 function of the skin depth $\delta = \sqrt{2/(\omega\mu\sigma)}$ for moderate to high conductivity values,

101 as follows:

$$\gamma = \sqrt{\omega^2 \mu (\epsilon_0 - j\sigma/\omega) - \beta^2} \quad (7)$$

$$\approx_{\sigma \gg \omega \epsilon_0} \frac{1-j}{\delta}. \quad (8)$$

102 The particular form of this wave number is responsible for the difficulties that arise
 103 in evaluating the interaction integrals (4)-(6) in a highly conductive medium. The
 104 Green's function in the conductor reduces to $\frac{j}{4} H_0^{(2)}((1-j)r/\delta)$, with $r = |\mathbf{r} - \mathbf{r}'|$,
 105 while its normal derivatives are expressible in terms of the zeroth, first and second
 106 order Hankel functions of the second kind (see appendix A). For large $|\gamma r|$, the
 107 Hankel function of the second kind and order ν behaves as [Watson, 1995]

$$H_\nu^{(2)}(\gamma r) \sim \left(\frac{2}{\pi \gamma r}\right)^{\frac{1}{2}} e^{-j\gamma r + j\frac{\pi}{4}(2\nu+1)} \quad (|\arg \gamma r| < \pi). \quad (9)$$

108 In a highly conductive medium, the large imaginary part of the wave number causes
 109 a strong exponential decay of the Green's function and its derivatives. Moreover,
 110 the wavelength $\lambda = 2\pi\delta$ is small w.r.t. the free space wavelength, which leads to
 111 a spatially strong oscillation of the Green's function and its derivatives. If S_j is a
 112 segment on the interface between the conductive region Ω and a dielectric region
 113 Ω_d , it is sufficient to choose the segment length to be a fraction of the wavelength
 114 λ_d in the dielectric, say $l_j = \frac{\lambda_d}{10} = \frac{2\pi}{10\omega\sqrt{\epsilon_d\mu_d}}$, in order to capture the varying field
 115 behavior at the interface. This is because the tangential fields at the interface can
 116 only vary at a pace on the order of λ_d in the dielectric and remain continuous at
 117 the interface (there are no surface currents). Typically $\delta \ll l_j$ and accordingly a
 118 lot of oscillations occur along one segment and standard quadrature techniques fail

119 to correctly evaluate the interaction integrals in the conductive region. Choosing
 120 $l_j = \frac{\lambda}{10}$ (with λ corresponding to the wavelength in the conductor) to try to tackle
 121 this problem is unnecessary to capture the field behavior and would lead to a very
 122 large increase of the number of unknowns.

5. Accurate Evaluation of MoM Interaction Integrals

123 This section proposes a new method to accurately evaluate the MoM interaction
 124 integrals in conductive media, with a relatively low quadrature order. The method
 125 reduces to the traditional approach in *Fostier et al.* [2011] for $\sigma \ll \omega\epsilon_0$ (low-loss
 126 dielectric case), and is therefore applicable to arbitrary conductivities $\sigma \in [0, \infty[$, as
 127 shown in this section and corroborated by the numerical examples in Section 6.

5.1. Cutoff Distance

128 The key to accurately integrate the strongly oscillating and exponentially decay-
 129 ing integrands in conductive media, for a fixed number of quadrature points, is to
 130 distribute those points over the integration domain where the Green's function has
 131 a non-negligible value. Because the magnitude of the Green's function decays ex-
 132 ponentially in a good conductor, it can be approximated as $\frac{j}{4}H_0^{(2)}(\gamma r)\mathbb{H}(r_{\text{cut}} - r)$,
 133 neglecting its tail, with \mathbb{H} the Heaviside step function and r_{cut} the cutoff distance.

134 The cutoff distance is the distance above which the asymptotic Green's function
 135 (using (9)) becomes smaller in magnitude than a threshold Δ_{cut} . It can be written
 136 in terms of the principal branch of the Lambert W function, denoted $\mathcal{W}(z)$.

Definition 1 (Cutoff distance r_{cut}).

$$r_{\text{cut}} = -\frac{1}{2\Im\gamma} \mathcal{W}\left(\frac{-4\Im\gamma}{\pi\Delta_{\text{cut}}^2|\gamma|}\right) \underset{\sigma \gg \omega\epsilon_0}{\approx} \frac{\delta}{2} \mathcal{W}\left(\frac{2\sqrt{2}}{\pi\Delta_{\text{cut}}^2}\right) \quad (10)$$

137 An upper bound on the Green's function itself is given in Theorem 5.1. For sufficiently
138 small Δ_{cut} , the asymptotic expansion (9) is a good approximation and $C \approx 1$.

139 **Theorem 5.1.** For $r \geq r_{\text{cut}}$ the following inequality holds: $|G(r)| \leq C\Delta_{\text{cut}}e^{(r-r_{\text{cut}})\Im\gamma}$

140 with $C = 1 + \frac{1}{8|\gamma|r_{\text{cut}}}$.

141 *Proof.* Note that $H_0^{(2)}(z) = \sqrt{\frac{2}{\pi z}} e^{-j(z-\frac{\pi}{4})} \left(1 - \frac{\theta_2(z)}{8jz}\right)$, with $|\theta_2(z)| < 1$ if $\Im z < 0$

142 [Gradshteyn and Ryzhik, 2007]. For $r \geq r_{\text{cut}}$, this leads to

$$\left|\frac{j}{4}H_0^{(2)}(\gamma r)\right| \leq \frac{1}{4}\sqrt{\frac{2}{\pi|\gamma|r_{\text{cut}}}} e^{r_{\text{cut}}\Im\gamma} e^{(r-r_{\text{cut}})\Im\gamma} \left(1 + \frac{1}{8|\gamma|r_{\text{cut}}}\right) \quad (11)$$

$$= C\Delta_{\text{cut}}e^{(r-r_{\text{cut}})\Im\gamma}, \quad (12)$$

143 where the last step follows from Definition 1. □

144 To illustrate the use of the cutoff distance in the calculation of the interaction
145 integrals, consider $\mathbf{l}_{jk}^{(1)}$ in a conductive medium:

$$\mathbf{l}_{jk}^{(1)} \approx \int_{S_j} p_j(\mathbf{r}) d\mathbf{c} \int_{S_k} G(\mathbf{r}|\mathbf{r}') \mathbb{H}(r_{\text{cut}} - |\mathbf{r} - \mathbf{r}'|) p_k(\mathbf{r}') d\mathbf{c}'. \quad (13)$$

146 The boundaries of the test integral over test segment S_j follow from the intersection
147 of S_j with the set of points that are closer than the cutoff distance from the source
148 segment S_k (region Υ_k in Fig. 3). Because Υ_k is convex, either $S_j \cap \Upsilon_k = \emptyset$
149 (no interaction) or $S_j \cap \Upsilon_k$ is a subsegment (AB in Fig. 3). For each test point
150 $\mathbf{r} \in (S_j \cap \Upsilon_k)$, the basis integration interval is a subsegment of S_k (CD in Fig. 4).

In this way, interactions between points that are separated further than r_{cut} are neglected and the quadrature points are distributed over the region where the in-

tegrand is non-negligible, which alleviates the problem of the exponential damping of the integrand. At the same time, the number of oscillations of the integrands in the interaction integrals is small, *independent of the conductivity*, allowing a relatively low quadrature order. To show this, consider an interface between free space (wavelength λ_0) and a conductive region (conductivity σ , wave number $\gamma = \sqrt{\omega^2 \mu_0 (\epsilon_0 - j\sigma/\omega) - \beta^2}$), with boundary segment length equal to $l = \lambda_0/10$. The integrands of the interaction integrals (4)-(6) can be expressed in terms of Hankel functions of the second kind, as shown in (15). For $\sigma \gg \omega \epsilon_0$, it is evident from (10) that $r_{\text{cut}} \sim \delta$, implying that the number of oscillations of $H_\eta^{(2)}(\gamma r)$ in $r \in [0, r_{\text{cut}}]$ is bounded for high conductivities. For $\sigma \ll \omega \epsilon_0$, $r_{\text{cut}} > l$ and the number of oscillations of $H_\eta^{(2)}(\gamma r)$ for $r \in [0, l]$ in a dielectric region is also bounded. A measure for the maximum number of oscillations of the integrands is given by

$$Z = \max_{\substack{\sigma \in [0, \infty[\\ \beta \in [0, \omega \sqrt{\epsilon_0 \mu_0}] \\ \eta \in \{0, 1, 2\} \\ \mathcal{P} \in \{\Re, \Im\}}} z(\mathcal{P}H_\eta^{(2)}(\gamma r), [0, \min(r_{\text{cut}}, l)]), \quad (14)$$

151 where $z(f(r), \mathcal{A})$ denotes the number of zero-crossings of $f(r)$ in $r \in \mathcal{A}$. It can
 152 be easily verified that $Z = 2, 4$ and 6 if $\Delta_{\text{cut}} = 10^{-3}, 10^{-6}$ and 10^{-9} , respectively,
 153 which shows that the number of oscillations increases if a higher accuracy is required
 154 (larger r_{cut}), but remains small, allowing a low quadrature order, independent of σ .
 155 In conclusion, the cutoff distance alleviates both problems of exponentially damped
 156 and highly oscillatory kernels in conductive media. This approach is an extension of
 157 the traditional method in *Fostier et al.* [2011], to accurately evaluate the interaction
 158 integrals in media with arbitrary conductivity.

5.2. Singularity Extraction

159 The three types of interaction integrals (4)-(6) can be written as

$$l_{jk}^{(l)} = \int_{C_i} w_j^{(l)}(\mathbf{r}) \int_{C_i} b_k^{(l)}(\mathbf{r}') \mathbb{H}(r_{\text{cut}} - r) \sum_{\eta=0}^2 f_{\eta}^{(l)}(\mathbf{r}, \mathbf{r}') H_{\eta}^{(2)}(\gamma r) dc' dc. \quad (15)$$

160 The test and basis functions are given by

$$w_j^{(1)}(\mathbf{r}) = w_j^{(2)}(\mathbf{r}) = p_j(\mathbf{r}), \quad (16)$$

$$w_j^{(3)}(\mathbf{r}) = t_j(\mathbf{r}), \quad (17)$$

$$b_k^{(1)}(\mathbf{r}') = p_k(\mathbf{r}'), \quad (18)$$

$$b_k^{(2)}(\mathbf{r}') = b_k^{(3)}(\mathbf{r}') = t_k(\mathbf{r}'). \quad (19)$$

161 As shown in appendix A, the functions $f_{\eta}^{(l)}(\mathbf{r}, \mathbf{r}')$ that are not identically zero are

162 given by

$$f_0^{(1)} = \frac{j}{4}, \quad (20)$$

$$f_1^{(2)} = \frac{j\gamma}{4}(\hat{\mathbf{n}}' \cdot \hat{\mathbf{r}}), \quad (21)$$

$$f_0^{(3)} = \frac{j\gamma^2}{8}(\hat{\mathbf{n}} \cdot \hat{\mathbf{n}}'), \quad (22)$$

$$f_2^{(3)} = \frac{j\gamma^2}{8} \left(\hat{\mathbf{n}} \cdot \hat{\mathbf{n}}' - 2(\hat{\mathbf{n}} \cdot \hat{\mathbf{r}})(\hat{\mathbf{n}}' \cdot \hat{\mathbf{r}}) \right). \quad (23)$$

163 If the test and basis functions' supports overlap or lie next to each other, the inte-

164 grands in (15) have a singularity in the integration domain. We employ a singularity

165 extraction technique with an extracted singular part that is also limited by the cutoff

166 distance, given by

$$l_{jk,\text{sing}}^{(l)} = \int_{C_i} w_j^{(l)}(\mathbf{r}) \int_{C_i} b_k^{(l)}(\mathbf{r}') \mathbb{H}(r_{\text{cut}} - r) \sum_{\eta=0}^2 f_{\eta}^{(l)}(\mathbf{r}, \mathbf{r}') \mathcal{S}_{\eta}(\gamma r) dc' dc. \quad (24)$$

167 The functions \mathcal{S}_η are given by

$$\mathcal{S}_0(\gamma r) = -\frac{2j}{\pi} \log r, \quad (25)$$

$$\mathcal{S}_1(\gamma r) = \frac{2j}{\pi \gamma r}, \quad (26)$$

$$\mathcal{S}_2(\gamma r) = \frac{4j}{\pi \gamma^2 r^2}. \quad (27)$$

168 The integrals of the limited singular parts are known in closed-form. For example,
 169 the self-patch term of the first type is given by

$$l_{jj,\text{sing}}^{(1)} = -\frac{j}{\pi} a((4l_j - 2a) \log a - 4l_j + a), \quad (28)$$

170 with $a = \min(r_{\text{cut}}, l_j)$.

6. Numerical Results

171 Plane wave scattering at a conductive cylinder is used to validate the accuracy of
 172 the proposed method as a function of the accuracy parameter Δ_{cut} , for a wide range
 173 of electrical conductivities in the general case of oblique incidence ($\beta \neq 0$), and to
 174 compare it with existing methods. The next examples are practically relevant shield-
 175 ing problems, in which a conductive and (non-)magnetic enclosure with apertures is
 176 used to shield the interior from the fields generated by an exterior electric current
 177 source. The new method is able to accurately calculate the shielding performance
 178 over a broad frequency range, and outperforms existing methods in terms of accuracy
 179 and simulation time.

6.1. Scattering at a Conductive Cylinder

180 To validate the accuracy of the proposed 2.5-D BEM for conductive media and
 181 compare it with existing numerical methods, we consider the problem of plane wave
 182 scattering at a conductive cylinder (diameter d , finite conductivity σ and permittivity
 183 $\epsilon_0 - j\sigma/\omega$), embedded in free space (Fig. 5). An analytical expression of the solution
 184 can be obtained via separation of variables [Van Bladel, 2007]. The accuracy of the
 185 proposed method is compared with the traditional method without cutoff distance,
 186 and with a surface impedance approximation, over a wide conductivity range, from
 187 the low-loss dielectric ($\omega\epsilon_0 \gg \sigma$) to the conductive region ($\omega\epsilon_0 \ll \sigma$).

188 The numerically obtained radar cross section (RCS), denoted $S_n(\phi)$, is compared
 189 with the analytical solution, denoted $S_a(\phi)$. The relative error between these cross
 190 sections is defined by

$$\mathcal{E} = \sqrt{\frac{\sum_{k=1}^K |S_n(\phi_k) - S_a(\phi_k)|^2}{\sum_{k=1}^K |S_a(\phi_k)|^2}}, \quad (29)$$

191 with $\phi_k = 2\pi k/K$ and $K = 100$. Figures 6-7 show the relative error as a function of
 192 the skin depth for the two polarizations (VV and VH) of oblique plane wave incidence
 193 ($\alpha = 45^\circ$). The skin depth $\delta = \sqrt{2/(\omega\mu_0\sigma)}$ ranges from 10^{-5} m to 10 m, covering
 194 the region between a good conductor with conductivity $\sigma = 10^7$ S/m and a low-loss
 195 dielectric with relative dielectric constant $1 - 5 \cdot 10^{-4}j$. Observe that, in general, the
 196 error decreases if the accuracy threshold Δ_{cut} becomes smaller. The relative error
 197 saturates around five significant digits for small and large skin depths, but this lower
 198 bound is determined mostly by the boundary meshing of the circular cross section
 199 into straight segments. The asymptotic value for the cutoff distance in (10), in case of

200 high conductivity, is shown in the legend. For $r_{\text{cut}} > d$, no interactions are neglected,
 201 and the numerical solution becomes independent of Δ_{cut} , as can be seen for high δ/d
 202 values.

203 The inability of the traditional method without cutoff distance (i.e. the proposed
 204 method with $r_{\text{cut}} = \infty$) to accurately evaluate the interaction integrals in conductive
 205 media, for a fixed quadrature order and constant number of boundary segments,
 206 is clearly demonstrated in Fig. 7. The problems mentioned in Section 4, i.e. the
 207 exponential decay combined with strong oscillation of the integrands, render the
 208 traditional method inaccurate or useless for low values of δ/d . The proposed method
 209 focuses the quadrature points in the region where the integrands are non-negligible,
 210 by introducing the cutoff distance (10) and a singularity extraction with limited
 211 extracted part, which in turn limits the number of oscillations. This leads to a near
 212 constant accuracy over the considered conductivity range (if enough oscillations are
 213 taken into account, i.e. for sufficiently low Δ_{cut}). For $r_{\text{cut}} > d$, or equivalently for
 214 high δ/d values, our new method reduces to the traditional one, and the numerical
 215 solution is the same for both methods.

216 Another approach to incorporate good conductors in a BEM is the use of a surface
 217 impedance approximation, by imposing the condition $\mathbf{E} \times \hat{\mathbf{n}} = Z_s(\hat{\mathbf{n}} \times \mathbf{H} \times \hat{\mathbf{n}})$ on
 218 the conductor boundary, with $Z_s = (1 + j)\sqrt{\frac{\omega\mu_0}{2\sigma}}$ and $\hat{\mathbf{n}}$ the outward normal to the
 219 conductive region. Figures 6-7 show that this is a good approximation for low values
 220 of δ/d , i.e. in the conductor skin-effect regime (note that the error does not saturate
 221 around 100 dB because the analytical solution with surface impedance approximation

is considered). It is apparent from Fig. 7 that the proposed method (with $\Delta_{\text{cut}} = 10^{-9}$) outperforms the surface impedance approximation and traditional method in terms of accuracy, in the transition region between low-loss dielectric and skin-effect regime.

6.2. Slotted Coaxial Shield

In this example, we investigate the shielding performance of a coaxial enclosure with one or two slots at angles α_1 and α_2 (Fig. 8). The coaxial enclosure is illuminated by an electric line current $I_0\delta(\mathbf{r} - \mathbf{r}_0)\hat{\mathbf{z}}$ (hence $\beta = 0$), which induces an unwanted noise current I_1 in the enclosed copper signal conductor. Remark that, in addition to our MoM integral equation technique, scattering at a concentrically loaded cylindrical shield with $n - 1$ apertures can be solved by reducing an n -series problem to an equivalent Riemann-Hilbert problem [Ziolkowski, 1985; Ziolkowski and Grant, 1987]. A similar radial mode matching technique has been employed for multi-slotted shields with finite thickness [Lee et al., 2012]. We consider three enclosure materials: copper ($\sigma = 5.8 \cdot 10^7$ S/m, $\mu_r = 1$), a magnetic conductor with the same skin depth ($\sigma = 5.8 \cdot 10^4$ S/m, $\mu_r = 1000$), and a perfect electric conductor ($\sigma = \infty$). The configurations with one and two slots are described by $\alpha_1 = 90^\circ$ and $(\alpha_1, \alpha_2) = (60^\circ, 120^\circ)$, respectively.

Figure 9 shows the relative noise current amplitude $|I_1/I_0|$ of the copper and perfect electric conducting (PEC) enclosure, over a broad frequency range (from 100 Hz to 1 GHz). Observe that the analytical solution for the closed coaxial enclosure (no slots) coincides with the numerical solution. At low frequencies, there is leakage

243 through the copper enclosure, as the skin depth is comparable to the thickness, and
244 the presence of slots does not deteriorate the shielding performance significantly. At
245 high frequencies, the predominant leakage mechanism is diffraction of the fields at
246 the slots, and the copper and PEC shields exhibit the same behavior. For the given
247 position of the slots and line current, the noise current for two slots is about 15 dB
248 higher than for one slot.

249 Figure 10 shows the relative noise current amplitude for the magnetic conducting
250 enclosure. For the configuration without slots, the numerical and analytical solution
251 coincide. Compared to the copper enclosure, at low frequencies, the presence of slots
252 now has a larger influence. This is due to a different shielding mechanism in the
253 magnetic conductor, adding to the effect of the conductivity. If $\mu_r > 1$, the magnetic
254 induction produced by the source is diverted into the enclosure, then shunted within
255 the material in a direction nearly parallel to its surface, and finally released back into
256 free space [Celozzi *et al.*, 2008]. The presence of slots disturbs the flux shunting, and
257 negatively affects the shielding performance.

258 It is interesting to compare our new method with the traditional method ($r_{\text{cut}} = \infty$)
259 in terms of accuracy and simulation time. Fig. 11 shows the calculated shielding
260 performance as a function of the quadrature order Q , for the copper shield with two
261 slots. For $\Delta_{\text{cut}} = 10^{-9}$, the new method already converges to the solution for $Q = 10$,
262 compared to $Q = 80$ for the traditional method. For the same quadrature order $Q =$
263 10, the traditional method fails to accurately predict the shielding performance, due
264 to the problems mentioned in Section 4. Evidently, the need for a smaller quadrature

265 order to obtain the same accuracy leads to a decrease in simulation time (Table
266 1). Even for the same quadrature order ($Q = 10$), our method is faster than the
267 traditional method because interactions between segments separated by at least the
268 cutoff distance are not taken into account.

6.3. Cable Tray Shield

269 The geometry of a metal cable tray with polygonal cross section (Fig. 12) is similar
270 to the previous example, but arguably more interesting from a practical perspective.
271 In this case, no closed-form analytical solution is available for the closed cable tray
272 ($g = 0$). The enclosure is illuminated by an electric line current $I_0\delta(\mathbf{r} - \mathbf{r}_0)\hat{\mathbf{z}}$ (hence
273 $\beta = 0$), which induces unwanted noise currents I_i in the three copper signal conduc-
274 tors. Figure 13 shows the relative current magnitude $|I_2/I_0|$ in the middle conductor,
275 for an open and closed cable tray (aperture length $g = 5.5$ mm and $g = 0$, respec-
276 tively). We consider three enclosure materials: copper ($\sigma = 5.8 \cdot 10^7$ S/m, $\mu_r = 1$), a
277 magnetic conductor with the same skin depth ($\sigma = 5.8 \cdot 10^4$ S/m, $\mu_r = 1000$), and a
278 perfect electric conductor ($\sigma = \infty$).

279 At low frequencies (up to 10^5 Hz), we notice that the influence of the apertures
280 can be neglected, as the open and closed cable tray yield approximately the same
281 shielding performance, for both copper and the magnetic conductor. In this region,
282 the skin depth is comparable to the thickness, allowing the fields to penetrate the
283 enclosure. At high frequencies, the copper and perfectly conducting open cable tray
284 behave in the same way, indicating that diffraction of the fields through the aperture

285 is the predominant leakage mechanism. Observe that the magnetic conductor exhibits
286 a worse shielding performance than copper, for all considered frequencies.

7. Conclusions

287 This paper presents a novel method to accurately and efficiently calculate 2.5-D
288 MoM interactions integrals in conductive media, with arbitrary permeability. The re-
289 sulting BEM is practically relevant to a large number of application domains, includ-
290 ing modal analysis of waveguides with non-perfect conductors, scattering problems,
291 and shielding problems with general three-dimensional sources.

Appendix A: Derivation of the Green's function's normal derivatives

Using the notation of Figure 14, the gradients of the Green's function $G(\mathbf{r}|\mathbf{r}') = \frac{j}{4}H_0^{(2)}(\gamma r)$ w.r.t. the observation point \mathbf{r} and source point \mathbf{r}' are given by

$$\nabla G(\mathbf{r}|\mathbf{r}') = -\nabla' G(\mathbf{r}|\mathbf{r}') = -\frac{j\gamma}{4}H_1^{(2)}(\gamma r)\hat{\mathbf{r}}. \quad (\text{A1})$$

From these expressions, the normal derivatives of the Green's function follow immediately:

$$\frac{\partial G}{\partial n}(\mathbf{r}|\mathbf{r}') = -\frac{j\gamma}{4}H_1^{(2)}(\gamma r)(\hat{\mathbf{n}} \cdot \hat{\mathbf{r}}), \quad (\text{A2})$$

$$\frac{\partial G}{\partial n'}(\mathbf{r}|\mathbf{r}') = \frac{j\gamma}{4}H_1^{(2)}(\gamma r)(\hat{\mathbf{n}}' \cdot \hat{\mathbf{r}}). \quad (\text{A3})$$

Taking the gradient w.r.t. \mathbf{r}' of (A1) leads to the following dyadic, with the dot representing the derivative of a holomorphic function:

$$\begin{aligned} \nabla' \nabla G(\mathbf{r}|\mathbf{r}') &= \nabla' \left(\frac{j\gamma}{4} \dot{H}_0^{(2)}(\gamma r) \right) \hat{\mathbf{r}} + \frac{j\gamma}{4} \dot{H}_0^{(2)}(\gamma r) \nabla' \hat{\mathbf{r}} \\ &= -\frac{j\gamma^2}{4} \ddot{H}_0^{(2)}(\gamma r) \hat{\mathbf{r}} \hat{\mathbf{r}} - \frac{j\gamma}{4r} \dot{H}_0^{(2)}(\gamma r) \hat{\phi} \hat{\phi}. \end{aligned} \quad (\text{A4})$$

After some manipulations, the second order normal derivative of the Green's function can finally be written as

$$\begin{aligned} \frac{\partial^2 G}{\partial n \partial n'}(\mathbf{r}|\mathbf{r}') &= \hat{\mathbf{n}}' \cdot \nabla' \nabla G \cdot \hat{\mathbf{n}} \\ &= \frac{j\gamma^2}{8} \left(H_0^{(2)}(\gamma r) + H_2^{(2)}(\gamma r) \right) \hat{\mathbf{n}} \cdot \hat{\mathbf{n}}' - \frac{j\gamma^2}{4} H_2^{(2)}(\gamma r) (\hat{\mathbf{n}} \cdot \hat{\mathbf{r}}) (\hat{\mathbf{n}}' \cdot \hat{\mathbf{r}}). \end{aligned} \quad (\text{A5})$$

Acknowledgments. This work is partially supported by the Research Foundation Flanders (FWO-V) and by BELSPO through the IAP Phase VII BESTCOM project. The data of the numerical examples can be obtained by contacting the corresponding

303 author. The authors are grateful to the editor and the anonymous reviewers for their
304 valuable comments.

References

- 305 Celozzi, S., R. Araneo, and G. Lovat (2008), *Electromagnetic Shielding*, Wiley Series
306 in Microwave and Optical Engineering, John Wiley & Sons.
- 307 Chakraborty, S., and V. Jandhyala (2004), Evaluation of Green's function integrals
308 in conducting media, *Antennas and Propagation, IEEE Transactions on*, 52(12),
309 3357 – 3363, doi:10.1109/TAP.2004.836430.
- 310 Chang, Y., and R. Harrington (1977), A surface formulation for characteristic modes
311 of material bodies, *Antennas and Propagation, IEEE Transactions on*, 25(6), 789
312 – 795, doi:10.1109/TAP.1977.1141685.
- 313 Coluccini, G., M. Lucido, and G. Panariello (2013), Spectral domain analysis of
314 open single and coupled microstrip lines with polygonal cross-section in bound and
315 leaky regimes, *Microwave Theory and Techniques, IEEE Transactions on*, 61(2),
316 736–745, doi:10.1109/TMTT.2012.2231424.
- 317 Dobbelaere, D., H. Rogier, and D. De Zutter (2013a), Properties and nu-
318 merical solutions of dispersion curves in general isotropic waveguides, *Mi-
319 crowave Theory and Techniques, IEEE Transactions on*, 61(9), 3161–3168, doi:
320 10.1109/TMTT.2013.2273760.
- 321 Dobbelaere, D., H. Rogier, and D. De Zutter (2013b), Accurate 2D MoM technique
322 for arbitrary dielectric, magnetic and conducting media applied to shielding prob-

- 323 lems, in *Electromagnetic Theory (EMTS), Proceedings of 2013 URSI International*
324 *Symposium on*, pp. 738–741.
- 325 Fostier, J., B. Michiels, I. Bogaert, and D. D. Zutter (2011), A Fast 2D Parallel
326 MLFMA Solver for Oblique Plane Wave Incidence, *Radio Science*.
- 327 Gradshteyn, I. S., and I. M. Ryzhik (2007), *Table of Integrals, Series and Products*,
328 *seventh edition*, Academic Press.
- 329 Graglia, R. (1993), On the numerical integration of the linear shape functions times
330 the 3-D Green’s function or its gradient on a plane triangle, *Antennas and Propa-*
331 *gation, IEEE Transactions on*, 41(10), 1448 –1455, doi:10.1109/8.247786.
- 332 Graglia, R., and G. Lombardi (2008), Machine precision evaluation of singular and
333 nearly singular potential integrals by use of Gauss quadrature formulas for rational
334 functions, *Antennas and Propagation, IEEE Transactions on*, 56(4), 981 –998,
335 doi:10.1109/TAP.2008.919181.
- 336 Khayat, M., and D. Wilton (2005), Numerical evaluation of singular and near-singular
337 potential integrals, *Antennas and Propagation, IEEE Transactions on*, 53(10),
338 3180 – 3190, doi:10.1109/TAP.2005.856342.
- 339 Lee, W.-S., H.-L. Lee, H.-S. Jang, H.-S. Tae, and J.-W. Yu (2012), Analysis of scat-
340 tering with multi-slotted cylinder with thickness: TM case, *Progress In Electro-*
341 *magnetics Research*, 128, 105–120.
- 342 Murphy, R. A., C. G. Christodoulou, and R. L. Phillips (1991), Electromagnetic
343 scattering from a finite cylinder with complex permittivity, *Proc. SPIE*, 1558, 295–
344 305, doi:10.1117/12.49635.

- 345 Olyslager, F., D. De Zutter, and K. Blomme (1993), Rigorous analysis of the propaga-
346 tion characteristics of general lossless and lossy multiconductor transmission lines
347 in multilayered media, *Microwave Theory and Techniques, IEEE Transactions on*,
348 *41*(1), 79–88, doi:10.1109/22.210232.
- 349 Peeters, J., I. Bogaert, and D. De Zutter (2012), Calculation of MoM interaction in-
350 tegrals in highly conductive media, *Antennas and Propagation, IEEE Transactions*
351 *on*, *60*(2), 930–940, doi:10.1109/TAP.2011.2173105.
- 352 Poggio, A., and E. Miller (1973), Integral equation solution of three-dimensional scat-
353 tering problems, in *Computer Techniques for Electromagnetics*, edited by R. Mittra,
354 chap. 4, Pergamon Press.
- 355 Polimeridis, A., and J. Mosig (2010), Evaluation of weakly singular integrals
356 via generalized cartesian product rules based on the double exponential for-
357 mula, *Antennas and Propagation, IEEE Transactions on*, *58*(6), 1980–1988, doi:
358 10.1109/TAP.2010.2046866.
- 359 Rao, S., D. Wilton, and A. Glisson (1982), Electromagnetic scattering by surfaces of
360 arbitrary shape, *Antennas and Propagation, IEEE Transactions on*, *30*(3), 409–
361 418, doi:10.1109/TAP.1982.1142818.
- 362 Tong, M., G. Pan, and G. Lei (2005), Full-wave analysis of coupled lossy transmission
363 lines using multiwavelet-based method of moments, *Microwave Theory and Tech-*
364 *niques, IEEE Transactions on*, *53*(7), 2362–2370, doi:10.1109/TMTT.2005.850438.
- 365 Van Bladel, J. (2007), *Electromagnetic Fields*, The IEEE Press Series on Electromag-
366 netic Wave Theory, second ed., Wiley.

- 367 Watson, G. (1995), *A Treatise on the Theory of Bessel Functions*, Cambridge Math-
368 ematical Library, Cambridge University Press.
- 369 Wilton, D., S. Rao, A. Glisson, D. Schaubert, O. Al-Bundak, and C. Butler (1984),
370 Potential integrals for uniform and linear source distributions on polygonal and
371 polyhedral domains, *Antennas and Propagation, IEEE Transactions on*, *32*(3),
372 276 – 281, doi:10.1109/TAP.1984.1143304.
- 373 Wu, T., and L. Tsai (1977), Scattering from arbitrarily-shaped lossy dielectric bodies
374 of revolution, *Radio Science*, pp. 709–718.
- 375 Yla-Oijala, P., and M. Taskinen (2003), Calculation of CFIE impedance matrix el-
376 ements with RWG and $n \times$ RWG functions, *Antennas and Propagation, IEEE*
377 *Transactions on*, *51*(8), 1837 – 1846, doi:10.1109/TAP.2003.814745.
- 378 Ziolkowski, R. (1985), n-Series problems and the coupling of electromagnetic waves to
379 apertures: A Riemann-Hilbert approach, *SIAM Journal on Mathematical Analysis*,
380 *16*(2), 358–378, doi:10.1137/0516026.
- 381 Ziolkowski, R., and J. Grant (1987), Scattering from cavity-backed apertures: The
382 generalized dual series solution of the concentrically loaded E-pol slit cylinder
383 problem, *Antennas and Propagation, IEEE Transactions on*, *35*(5), 504–528, doi:
384 10.1109/TAP.1987.1144143.

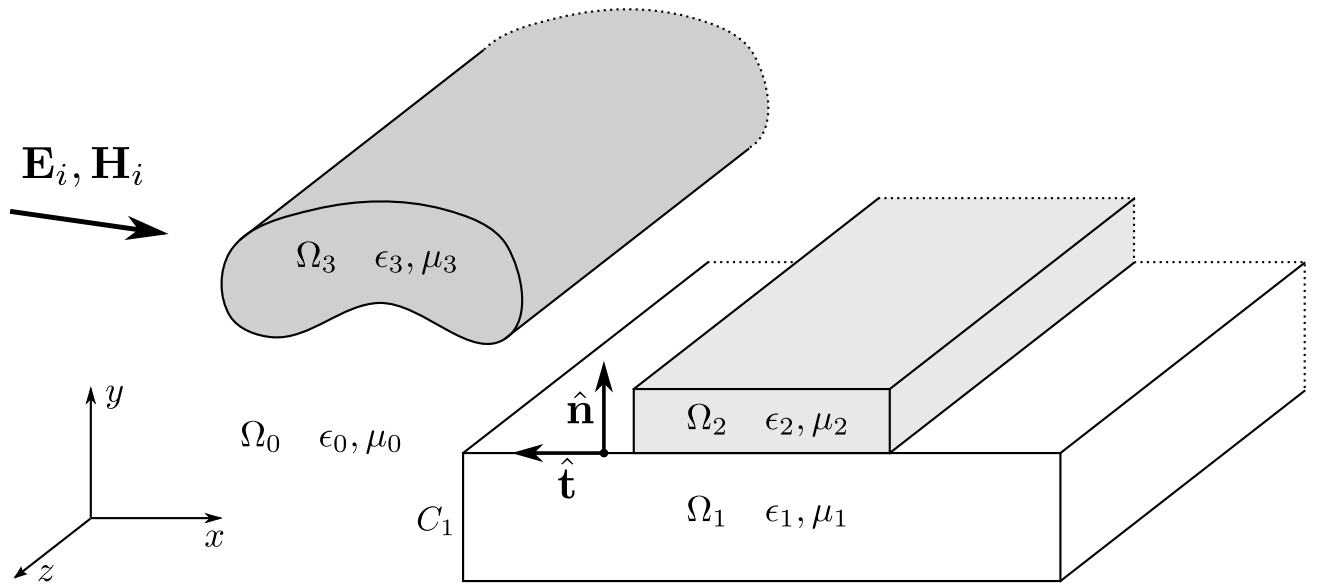


Figure 1. General isotropic piecewise-homogeneous 2-D geometry with a 3-D excitation.

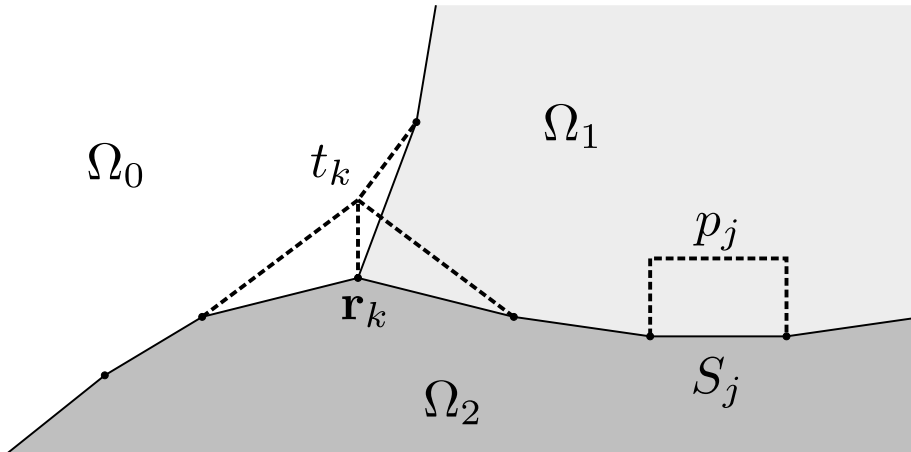


Figure 2. The boundaries are approximated with straight segments along which triangular and pulse functions are defined.

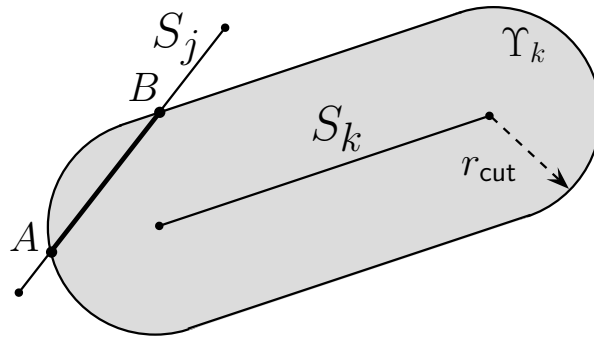


Figure 3. Test integration interval AB, where the interactions from segment S_k are non-negligible.

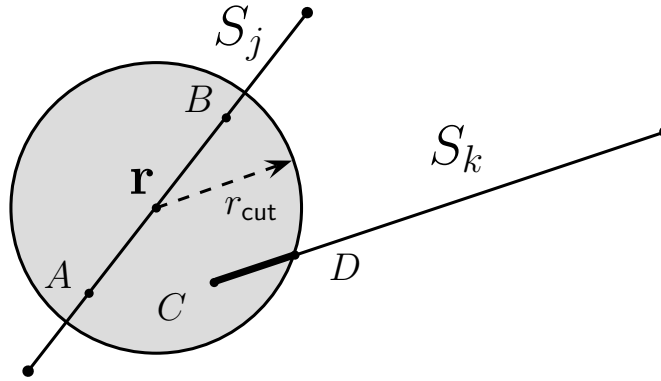


Figure 4. Basis integration interval CD , for test point \mathbf{r} .

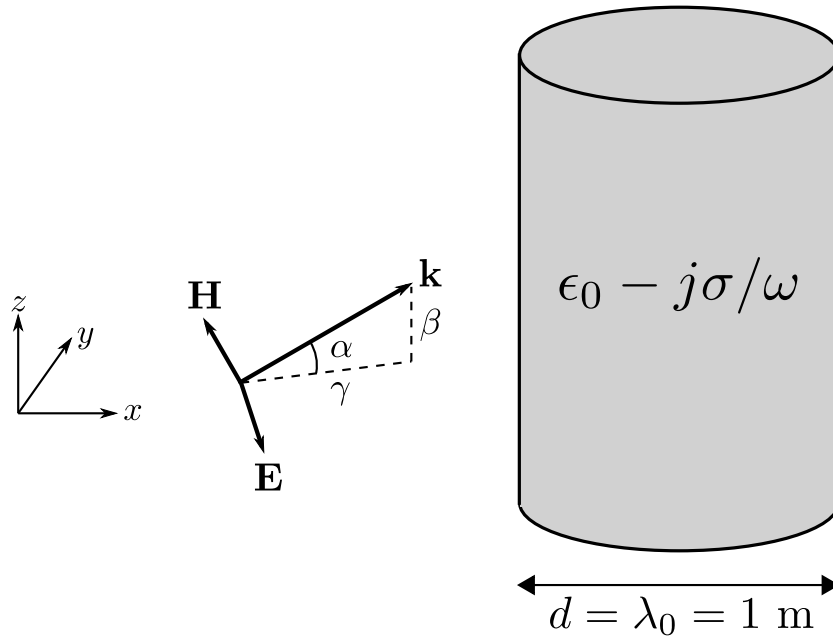


Figure 5. Plane wave scattering at a conductive cylinder with conductivity σ , permittivity $\epsilon_0 - j\sigma/\omega$ and diameter $d = 1$ m. The cylinder is illuminated by a linearly polarized plane wave, with free space wavelength $\lambda_0 = 1$ m, impinging at an angle α w.r.t. the (x, y) plane.

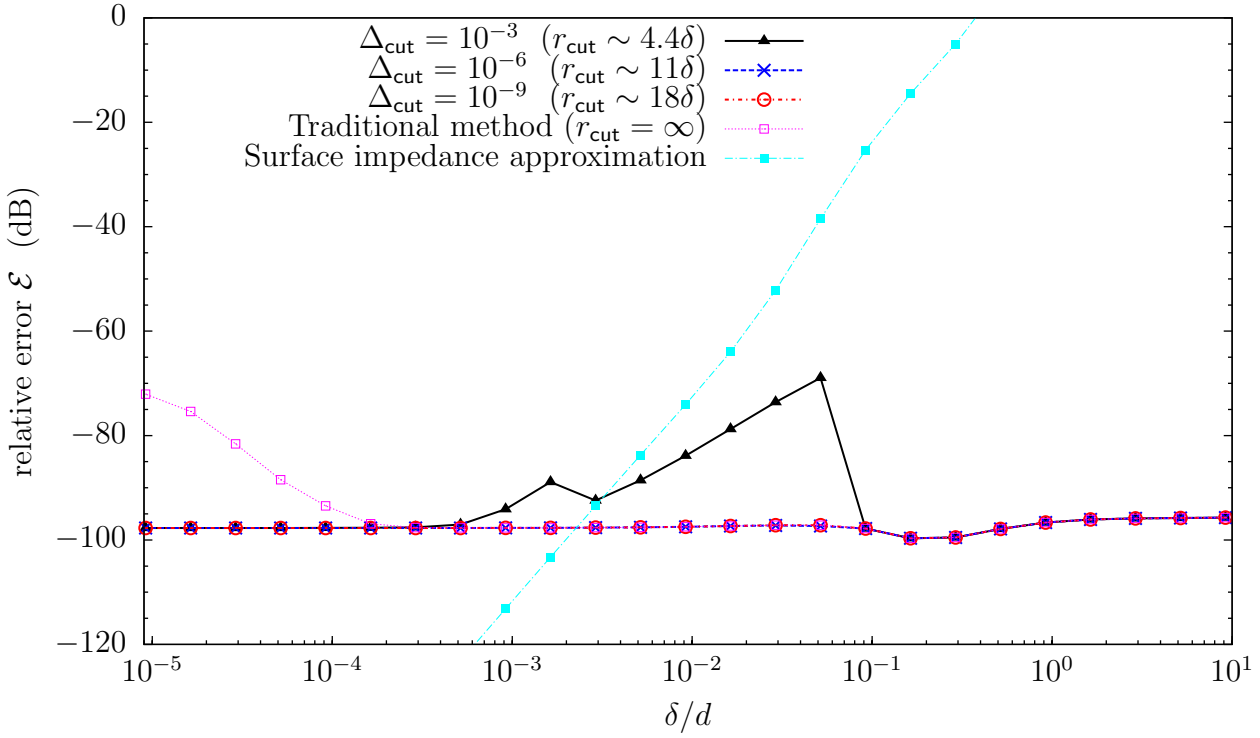


Figure 6. Relative error of the co-polarization RCS (VV) as a function of the skin depth δ for oblique incidence ($\alpha = 45^\circ$) for the proposed method, the traditional method without cutoff distance and limited extracted part, and a surface impedance approximation. The quadrature order of the interaction integrals ($Q = 32$) and number of boundary segments ($N = 630$) are constant.

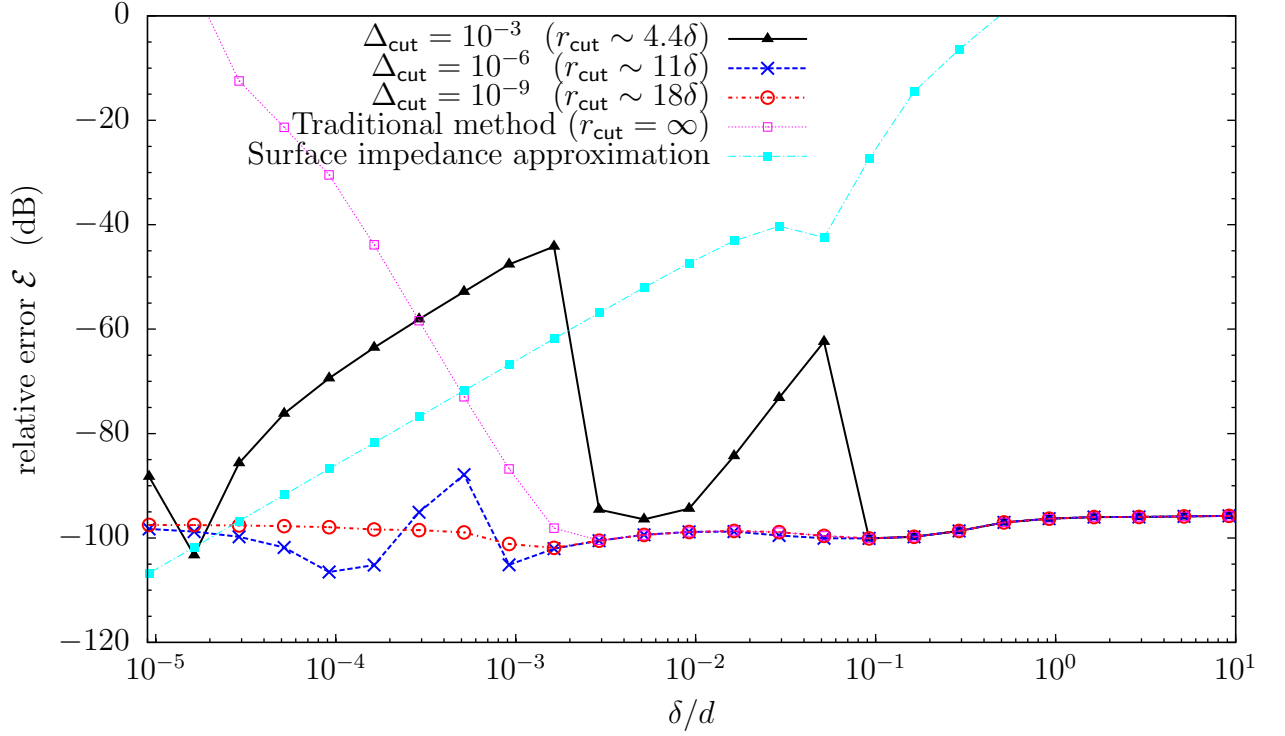


Figure 7. Relative error of the cross-polarization RCS (VH) as a function of the skin depth δ for oblique incidence ($\alpha = 45^\circ$) for the proposed method, the traditional method without cutoff distance and limited extracted part, and a surface impedance approximation. The quadrature order of the interaction integrals ($Q = 32$) and number of boundary segments ($N = 630$) are constant.

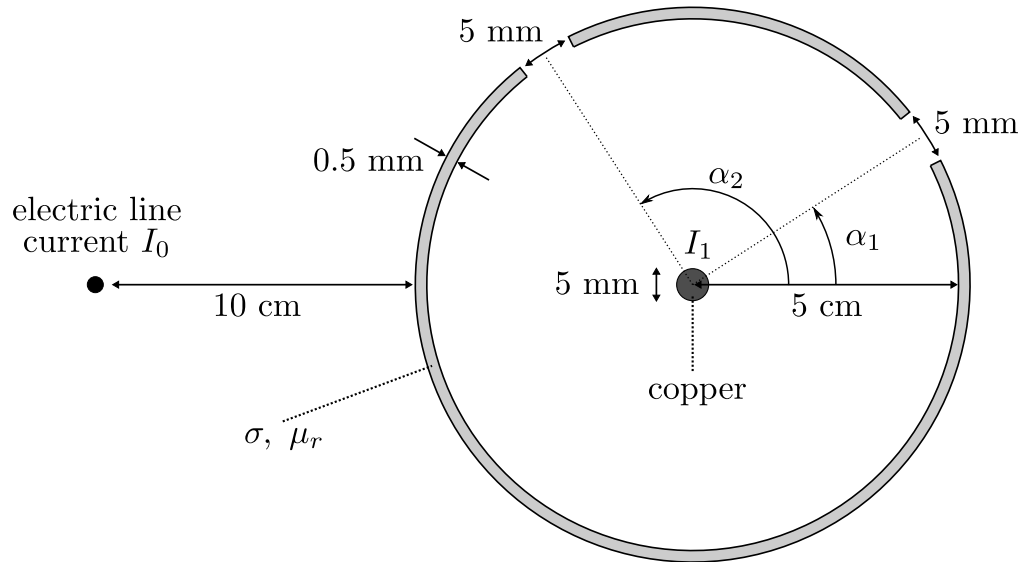


Figure 8. Cross section of a coaxial enclosure with conductivity σ and relative permeability μ_r , illuminated by an electric line current I_0 , and enclosing a copper signal conductor with induced noise current I_1 . There are one or two slots present at angles α_1 and α_2 .

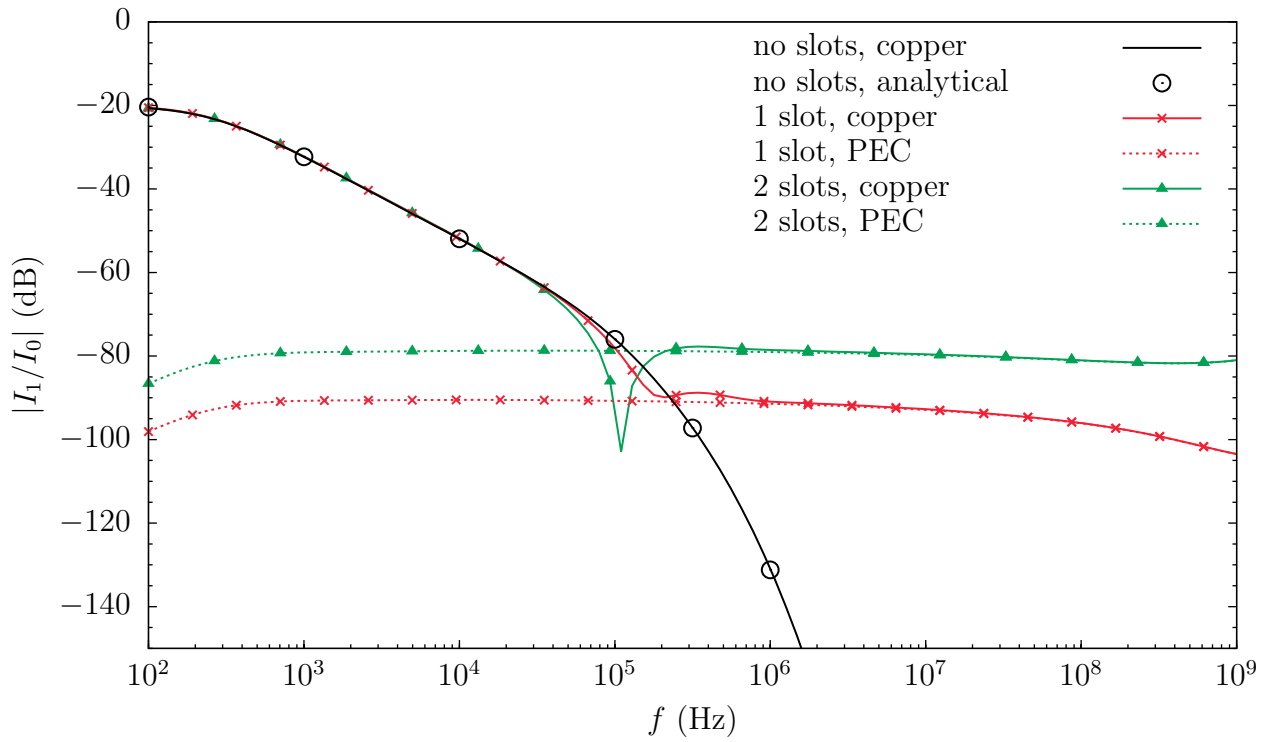


Figure 9. Shielding performance of the coaxial enclosure as a function of frequency, for a copper and perfect electric conducting (PEC) enclosure, with a varying number of slots.

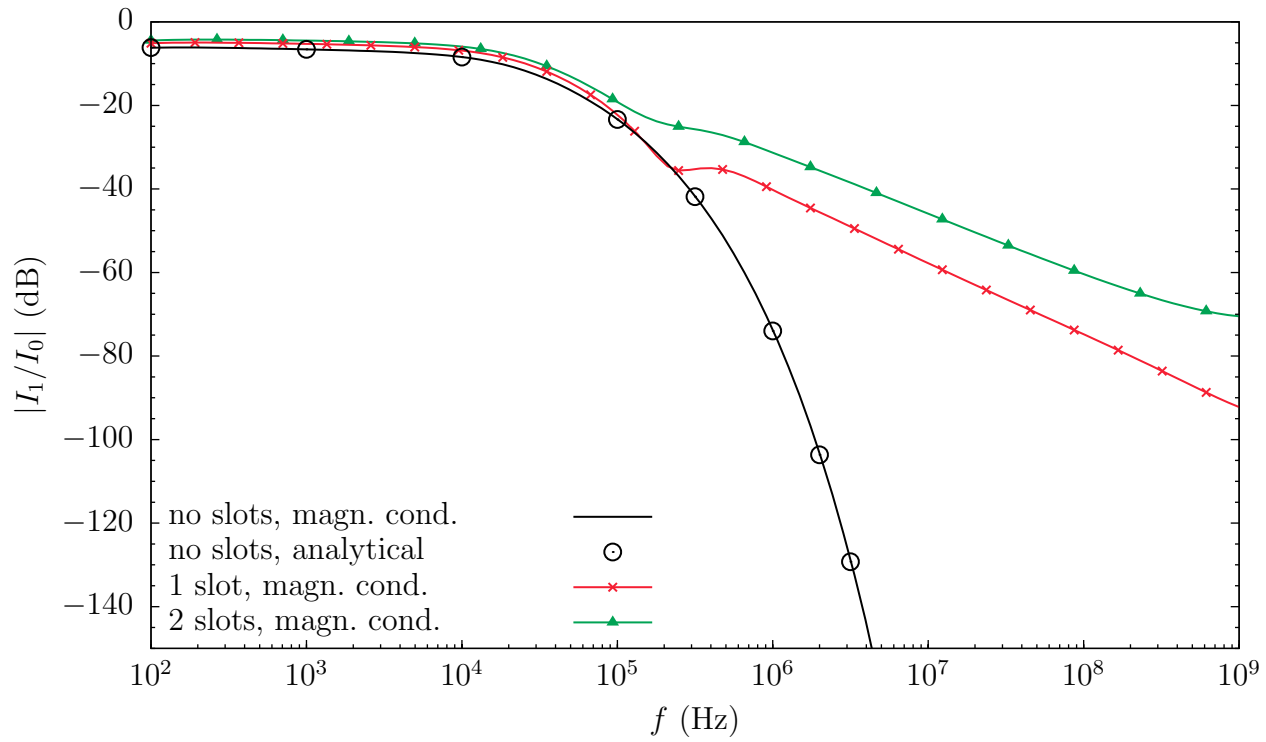


Figure 10. Shielding performance of the coaxial enclosure as a function of frequency, for the magnetic conductor, with a varying number of slots.

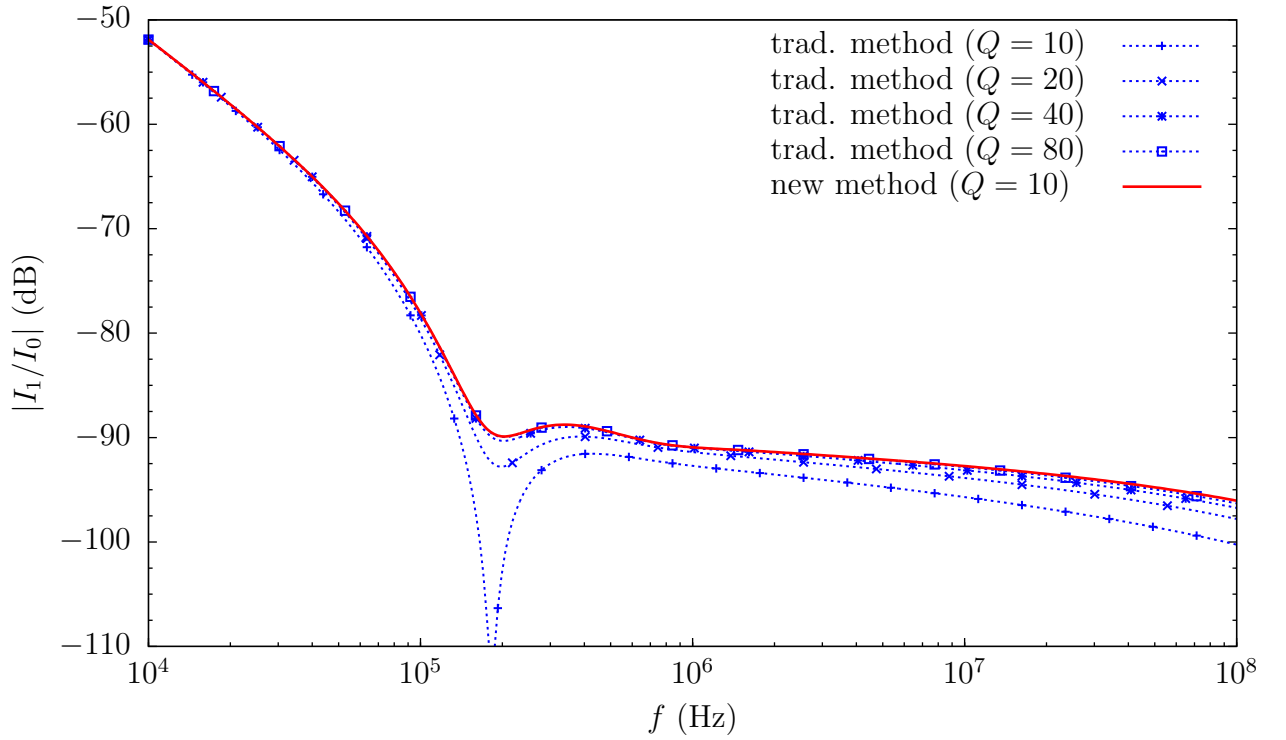


Figure 11. Comparison between the traditional method (with $r_{\text{cut}} = \infty$) and the new method in this work (with $\Delta_{\text{cut}} = 10^{-9}$), of the calculated shielding performance of the copper coaxial enclosure with two slots, for a varying quadrature order Q .

Table 1. Simulation time of the new method (top) and the traditional method (bottom), versus the quadrature order Q (see Fig. 11).

Q	Time (s)
10	10
10	17
20	45
40	150
80	575

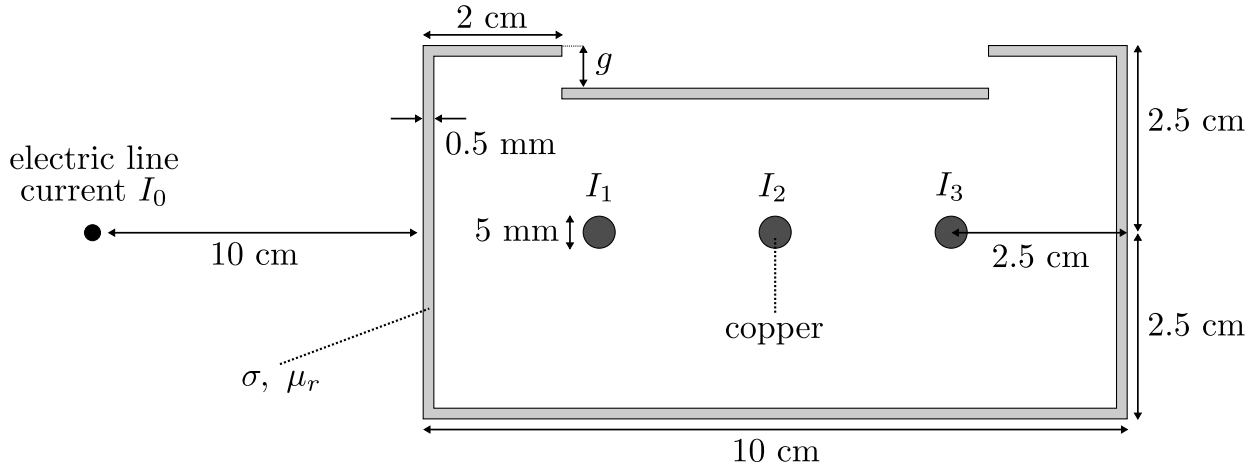


Figure 12. Cross section of an open cable tray with conductivity σ and relative permeability μ_r , illuminated by an electric line current I_0 , and enclosing three copper signal conductors with induced noise currents I_1 to I_3 . The geometry is symmetrical w.r.t. a vertical line through the center of the middle conductor.

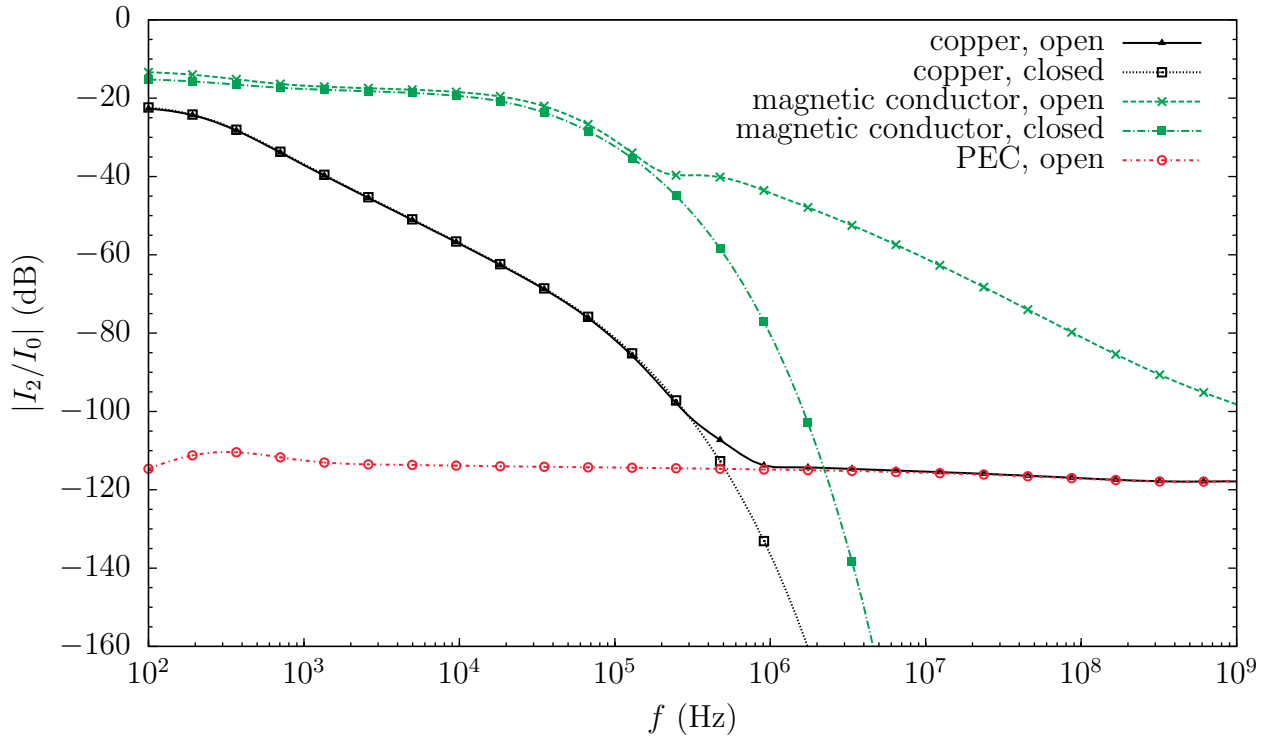


Figure 13. Shielding performance of the open ($g = 5.5$ mm) and closed ($g = 0$) cable tray as a function of frequency, for various shielding materials.

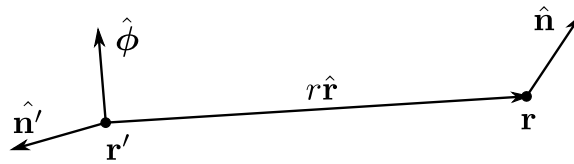


Figure 14. Relevant to the derivation of the normal derivatives.